Musculoskeletal Modelling and Predictive Simulation of Baseball Pitching to Improve Performance and Mitigate Injury Using Forward Dynamics and Optimal Control

Cedric E. Attias[1,3*], Thomas K. Uchida[2], Keaton Inkol[3,4], John McPhee[4]

[1]Mechanical Engineering, University of Waterloo, 200 University Avenue West, Waterloo, Ontario, N2L 3G1, Canada.
[2]Mechanical Engineering, University of Ottawa, 161 Louis-Pasteur, Ottawa, Ontario, K1N 6N5, Canada.
[3]Data Science, Seattle Mariners, 1250 1st Avenue South, Seattle, Washington, 98134, USA.
[4]Systems Design Engineering, University of Waterloo, 200 University Avenue West, Waterloo, Ontario, N2L 3G1, Canada.

*Corresponding author(s). E-mail(s): cattias@uwaterloo.ca;
Contributing authors: thomas.uchida@uottawa.ca;
kainkol@uwaterloo.ca; mcphee@uwaterloo.ca;

Abstract

An optimized forward dynamic model of baseball pitching was developed to assess muscle contributions to valgus torque on the elbow, with the goal of minimizing ulnar collateral ligament loads without compromising ball speed. A musculoskeletal model was created in OpenSim 4.5 to replicate the motion of Major League Baseball pitchers, incorporating the muscles responsible for resisting or producing valgus moments, which are known to affect ulnar collateral ligament loads. Using an optimal control framework in OpenSim Moco, muscle activations and actuator contributions were evaluated at various pitch speeds. Results demonstrated how optimized pitching motions differed from traditional techniques, suggesting kinematic adjustment strategies to reduce ligament load. For instance, faster pitches exhibited greater contralateral trunk tilt and higher arm slot, while slower pitches demonstrated greater ipsilateral trunk tilt with a lower arm slot (sidearm).

These findings show the potential of our methods to provide actionable insights into injury prevention for pitchers by identifying movement modifications that can reduce loads on the ulnar collateral ligament while maintaining competitive pitching speeds. By presenting a novel predictive simulation of baseball pitching, this work demonstrates the balance between performance and injury mitigation through biomechanical modelling and optimization, which can be transferred into player training strategies.

Keywords: Baseball, Injury, Optimal Control, Pitching, Predictive Simulation, Ulnar Collateral Ligament

1 Introduction

Professional baseball pitching is a complex, high-speed motion that places significant biomechanical demands on the body, particularly the elbow joint. The ulnar collateral ligament (UCL) is highly susceptible to injury during pitching due to the extreme valgus torques experienced during the arm-cocking and acceleration phases of the pitch [1, 2]. These ligament loads are amplified by the explosive movement of the shoulder and elbow [1, 3]. UCL injuries have become increasingly prevalent among elite pitchers and often require surgical intervention to reconstruct the ligament (i.e. Tommy John surgery), which can result in long recovery times and can impact career longevity.

Given the growing concern over UCL injuries, there is a critical need for methods to optimize pitching mechanics in a way that reduces ligament loads while maintaining competitive performance. Traditional approaches to injury prevention often focus on limiting pitch counts or adjusting training regimens, but these methods do not directly address the mechanics of the pitching motion and usually require physical testing of the athletes [4]. A promising alternative is to use biomechanical modelling and optimization to develop pitching techniques that balance performance with injury mitigation, without imparting undue workloads on the pitcher.

The purpose of this study is to develop a forward dynamic model of professional baseball pitching using OpenSim, an open-source musculoskeletal modelling software [5]. The forward dynamic approach differs from traditional inverse kinematic analyses in that it uses muscle-driven simulations to predict optimal motion based on applied forces and joint dynamics [6–8]. The model constructed in this study aims to replicate the anatomical features and capabilities of a Major League Baseball (MLB) pitcher, focusing specifically on the muscles responsible for resisting or generating valgus moments at the elbow [9]. Unlike previous research that relies on kinematic tracking of experimental pitching data, this study uses optimal control theory to predict novel pitching motions [6, 7]. This strategy discovers the optimal muscle activations and joint motions required to minimize UCL loading without compromising ball speed [1, 3].

The novelty of this work lies in the combination of musculoskeletal modelling, optimal control, and a focus on minimizing injury risk without compromising performance [10]. Unlike models that rely heavily on input data from athlete motions,

this work predicts motions that are optimized for a combination of performance and safety. We simulated several pitching scenarios, including standard MLB-level pitch speed and extreme conditions, to understand how unique simulated kinematic adjustments could alter UCL loading [1–3]. The results highlighted mechanical differences between optimized and traditional pitching techniques, particularly in the tilt of the trunk and shoulder abduction. For instance, increasing ipsilateral trunk tilt and lowering the arm slot substantially reduced valgus moment, although these changes came at the expense of reduced ball speed; in contrast, pitches with greater ball speeds had greater contralateral trunk tilt and a higher arm slot [1, 3].

2 Methods

A musculoskeletal model was developed using OpenSim 4.5, an open-source software for creating and analyzing biomechanically accurate musculoskeletal models of human movement [5]. The model was based on a validated open-source model, which we modified to better represent the anatomy of an elite MLB pitcher (see Section 2.1). Key modifications included the removal of kinematic joint coupling constraints, the inclusion of relevant muscles involved in valgus moment production, the addition of reserve actuators to supplement the muscle-generated joint moments, and the use of primary actuators to drive joint coordinates that were not actuated by muscles (i.e. all joints except those of the throwing arm). Ligaments were also removed from the original model.

The model was designed through a series of pre-processing steps, which used 43 fastball pitches that were recorded using markerless motion capture from a single starting MLB pitcher during a single game, and were anonymized and shared by KinaTrax (Boca Raton, FL, USA). Each set of pitching data contained transformation matrices at each time point (300 Hz) for each tracked body segment. All pitches were four-seam fastballs. The pre-processing steps for the forward dynamic analysis relied on inverse kinematic and inverse dynamic analyses of these 43 pitches, which were extracted using custom Visual3D kinematics and kinetics pipelines, respectively. Visual3D was used since it integrates directly with KinaTrax motion capture data to build a custom musculoskeletal model. Consistency across the Visual3D model and forward dynamic model was maintained by extracting the subject-specific anthropometric and inertial properties of the model from Visual3D and using them to design the OpenSim forward dynamic model. Joint trajectories, in the form of Euler angles, from the 43 pitches were averaged from the inverse kinematic analyses and used to define the OpenSim model's initial pose, inform the joint motion limits, and provide joint trajectory initial guesses for the optimization. Peak net joint forces and torques were extracted from the inverse dynamic analyses, averaged over the 43 pitches, and used to define the peak optimal torques of the musculoskeletal model's actuators. The initial pose, joint motion bounds, and actuator peak torque values used in the musculoskeletal model can be found in Appendix A. The inputs from the inverse kinematic and inverse dynamic analyses serve to better approximate the performance capabilities of an elite pitcher, compared to the default model's performance capacity. The model's starting pose was set at the instant of peak lead knee height and simulations proceeded to ball

release, as this interval represents the most strenuous portion of the pitching motion [1, 11–13]. The motion duration, spanning from peak lead knee height to ball release, was 0.7 s, averaged over the inverse kinematic analyses; simulation completion bounds were set to between 0.4 s and 1.0 s to align with literature values [14].

Consistency between Visual3D and OpenSim in our workflow was ensured by exporting motion that was expressed in OpenSim's joint space, axes, and constraints, as described in the Visual3D documentation [15]. Specifically, Visual3D (i) computes subject-specific segment scale factors and writes them to an OpenSim scaling file, (ii) performs inverse kinematics against the OpenSim gait model to fit both the static calibration trial and the dynamic trial, and (iii) outputs an OpenSim-ready .mot file that obviates the need to re-run OpenSim's Scale and IK Tools. Thus, what OpenSim received from Visual3D was a kinematic solution conforming to OpenSim's own joint definitions. We then used subject-specific inertial properties derived from the same source to build the forward model, preserving parent–child frames and mass properties across platforms. Together, these steps maintained cross-platform consistency in poses and loads despite differences in platform-specific angle parameterizations.

In the remainder of this section, details of the model revisions aimed at improving simulated pitching plausibility are given, including adjustments to the musculoskeletal model, muscle and actuator architecture, joint ranges of motion (ROM), and the modelling of the baseball and ground reaction forces (GRF).

2.1 Musculoskeletal Model of Pitching

The base musculoskeletal model used in this research was adapted to reflect the physical characteristics and capabilities of a professional pitcher. In OpenSim model development, it is common to adapt existing models for specific use cases [16]. This study required a model with full-body anatomy, including bones and muscles relevant to valgus loading on the UCL of the throwing arm. Since no validated open-source model exists for dynamic athletic motions like baseball pitching, the open-source "Upper and Lower Body Model" was chosen as the base model. This model combines lower-limb components from Delp et al. and upper-limb components from Holzbaur et al., including bones and most muscles with validated musculoskeletal dynamics [5, 9, 10, 17–20].

In the original model developed by Holzbaur et al. [18], the thoracolumbar orientation was defined following the International Society of Biomechanics (ISB) convention with the 3 degrees of freedom (DOF) being the plane of elevation, elevation, and axial rotation. Using this parameterization, shoulder flexion and abduction are not independent DOFs; rather, they are the sagittal- and frontal-plane components of a single elevation magnitude, coupled through the plane-of-elevation angle. This coupling compactly represents shoulder motion and is consistent with how clinicians describe scapulohumeral rhythm. For the present work, all joint coupling was removed to simplify the motion of the shoulder and we instead reported shoulder flexion, abduction, and rotation directly, which are more commonly used in the analysis of baseball pitching. Practically, we edited the thoracohumeral joint's coordinate set with a custom 3-DOF ball joint (via a *CustomJoint*/*SpatialTransform* in OpenSim). The new

joint defined three independent rotational coordinates named *shoulder_flexion*, *shoulder_abduction*, and *shoulder_rotation*, each applied about anatomically meaningful axes in the parent/child (thorax/humerus) frames, with an X-Y-Z rotation sequence, corresponding to flexion/extension (X), abduction/adduction (Y), and axial rotation (Z) of the shoulder. This X-Y-Z sequence provided the most comparable and realistic joint angles when compared to literature [21]. The rotation sequence was selected in Visual3D during the inverse kinematic analysis pre-processing stage [22]. We acknowledge that this decoupling may cause deviations when compared to the native ISB description presented by Holzbaur et al. (e.g., changes in the planes of motion of the 3-DOF joint at the shoulder), but it improves reproducibility and domain relevance in baseball applications. Muscle paths, objects around which muscles wrap, and rigid-body inertial properties were retained from the original model of Holzbaur et al.

The base model was also adapted to meet the demands of MLB pitchers, as follows. Muscles not relevant to this study were removed. Joint motion coupling constraints were removed to permit the ROM expected in elite pitchers, with the bounds of the ROM informed by the inverse kinematic analyses of 43 pitches (described above). Fifteen muscles were identified as resisting or producing valgus moments at the elbow during pitching and were retained: pronator teres (PT), flexor carpi radialis (FCR), flexor carpi ulnaris (FCU), palmaris longus (PL), four flexor digitorum superficialis muscles (FDSL, FDSR, FDSM, FDSI), biceps (BIClong, BICshort), triceps (TRImed, TRIlat, TRIlong), anconeus (ANC), and brachialis (BRA) [10, 23–25]. Muscle paths were not changed and all ligaments were removed.

A baseball with appropriate dimensions and inertial properties was rigidly connected to the right (throwing) hand at the base of the second metatarsal, reflecting a fastball grip. The baseball was designed with a mass of 0.145 kg, a radius of 0.0364 m, and principal moments of inertia of 7.68×10^{-5} kg·m^2 (modelled as a solid sphere) with the centre of mass being located at the centre of the ball.

A pre-processing step was conducted to scale the model's dimensions to match those of a typical MLB starting pitcher (height 6'3" or 1.905 m, weight 215 lb or mass 97.5 kg). Scaling was performed using OpenSim's *Scale Tool*, which adjusted the segment lengths and mass properties to match the anthropometry of the pitcher [5]. The OpenSim *Scale Tool* updates the dimensions of a model to match a particular individual by minimizing the error between experimental marker position data and markers placed on the musculoskeletal model [5]. Integration between Visual3D and OpenSim permitted direct scaling of body segments using the dimensions of the Visual3D model, which were already scaled to the individual pitcher. Specifically, a set of scale factors (multipliers) representing the relative scale of the Visual3D model's segments to those of the OpenSim model was generated. Inputting the scale factors and the desired height and mass of the model into the *Scale Tool* produced a model with the desired proportions and body segment mass properties.

The muscle models used in this research employed the Millard 2012 Equilibrium Muscle Model, a Hill-type muscle model that estimates muscle force generation assuming that the muscle fibers and tendon remain in equilibrium [26]. Reserve actuators were added to supplement the force-generation capabilities of the muscles, ensuring that the model could generate sufficient joint moments during the pitching motion

[10, 27]. The remaining joints, without the support of muscles, were driven by primary actuators. Actuator peak torques were extracted from the inverse dynamic analyses conducted in Visual3D (Appendix A).

Some muscle parameters were adjusted to better reflect the athletic capabilities of an elite pitcher; these changes were informed by literature [7, 10, 28, 29]. Muscle maximum isometric forces were increased by 30% from their default values in the base model, as outlined in papers by Buffi et al. and Hortobágyi and Katch [7, 28]. Hortobágyi and Katch [28] examined peak net joint torques in low- and high-strength populations and found that, on average, the high-strength group had a 25% greater peak net torque in elbow flexion and elbow extension than the low-strength group. Buffi et al. assumed that this difference in peak net joint torque was due to a proportionate increase in maximum isometric force, but further increased the maximum isometric force to 30%, presumably to model a collegiate athlete population with greater-than-average joint torques (though this is not stated explicitly) [7]. One would expect a professional athlete population to have even greater maximum isometric forces than a collegiate population; however, the expected increase is speculative and requires experiments to calibrate. For consistency with the work of Buffi et al., we also increased the maximum isometric forces in the original model by 30%. Reserve actuator maximum torques were also increased by 30%, but with respect to the mean peak torques extracted from the inverse dynamic analyses in Visual3D. Namely, peak throwing shoulder rotation actuation was set to 450 N·m, shoulder abduction/adduction and horizontal flexion/extension actuation were also set to 450 N·m, elbow flexion/extension and pronation/supination actuation were set to 350 N·m, and wrist flexion/extension and deviation were set to 300 N·m and 120 N·m, respectively. Primary actuator maximum torques were doubled with respect to the mean peak torques for their respective joints determined from the inverse dynamic analyses in Visual3D. Primary actuators were assigned higher peak torques than reserve actuators because the joints that they actuate do not have any modelled muscles to support the generation of motion. These changes were informed by Hortobágyi and Katch [28] and Buffi et al. [7]. Optimal fiber lengths and tendon slack lengths were scaled using the multipliers identified from the model scaling process for their respective body segments. The muscle activation time constant was reduced from 0.01 s to 0.005 s and the maximum normalized force achievable during eccentric contraction (force–velocity multiplier) was increased from 1.4 to 1.8, as outlined by Buffi et al. [7]. The halving of the muscle activation time constant was informed by a review of literature examining the sensitivity of Hill-based muscle models to perturbations in model parameters, where it was found that 0.005 s was the lower bound of commonly used values in the literature whereas 0.01 s was the upper bound [30]. The lower bound was selected to better represent the high speed of the pitching motion.

The final model included 34 DOF, with each joint actuated either by muscles with reserve actuators or by primary actuators. The pelvis served as the root segment of the model with 6 DOFs relative to the ground (3 translations, 3 rotations). The joint limits were modified to allow for a full ROM that is typically seen in elite pitchers, which surpasses the bounds of average joint ranges included in the default model [9].

The ROM bounds were relaxed by ±10% on each end based on mean joint angle trajectories from Visual3D. The joint DOF and ROM are tabulated in Appendix A.

GRFs were modelled using contact spheres in OpenSim, which were placed on the leading (left) foot to simulate interactions with the ground during pitching [5, 17, 31]. Two contact spheres were used with one fixed to the calcaneus at the heel and one fixed to the toes at the ball of the foot, with radii 0.03 m and 0.015 m, respectively. The stiffness, damping, and friction properties of these contact spheres were based on those used in previously validated gait models [5]. The height of the mound was ignored in this study for simplicity, resulting in a flat lead-foot contact with the ground (whereas the inclusion of a mound would result in a declined lead-foot contact). We acknowledge that more than two contact spheres have been used in previous predictive simulations of three-dimensional movement [32, 33]. The balance and stability of our model could be compromised with the use of only two contact spheres, potentially affecting the model's kinematics. We used only two spheres because our simulations began at peak lead knee height, where the lead foot was suspended in the air and made contact with the ground only briefly at the end of the simulation (the lead foot was in the air for 87.3%, 86.7%, and 83.6% of the simulation duration for Cases 1–3, respectively). Using two contact spheres improved Moco's convergence and numerical stability for our simulation goals. Additional spheres would have introduced additional contact states and controls, increasing computation time. With only two contact spheres, the Jacobians/Hessians were smaller and better conditioned, accelerating line searches and reducing solver chatter. Because Moco (via *CasADi*) relies on smooth derivatives, fewer simultaneous contacts with *SmoothSphereHalfSpaceForce* also produce cleaner sensitivities, since there are fewer overlapping sharp force ramps, improving the performance of the adjoint/auto-differentiation algorithm. Ultimately, this is a limitation of the present study. In future work, we will increase the number of spheres on the lead foot, calibrate the contact model parameters, and validate against experimentally collected force-plate GRFs to more faithfully reproduce stance-phase mechanics while maintaining solver stability.

The right (rear) foot was attached to the ground using a point constraint that enforced coincidence between a point on the distal end of the third metatarsal and a fixed point on the ground. This modelling simplification avoided the use of contact spheres on the right foot, which decreased computation time dramatically. In OpenSim, a point constraint prohibits relative translation between the two constrained points while permitting relative rotation about all three axes [34]. As such, this constraint is appropriately classified as a spherical (ball-and-socket) joint. The ROM of the ankle and subtalar joints were selected and enforced to ensure that the motion permitted via the spherical joint did not cause the foot to pass through the ground (see Appendix A). The constraint was placed specifically at this location to permit both the pivoting and heel lift expected at ball release during a pitch (see Fig. 2). The lift of the rearfoot heel was achieved through a combination of ankle flexion/extension and subtalar movement via inversion/eversion (see Appendix A). The assumption that the rear foot remained in contact with the ground through ball release was a simplification that was mechanically consistent with our simulation horizon (i.e. ending at ball release) and is supported by recent evidence on leg-specific impulse generation. In particular, Liu et

al. [35] reported that the rear leg generates substantial positive angular impulse while the rear foot is in contact with the ground at ball release, with only a small backward (braking) linear impulse. These contact forces produce a ground reaction moment that helps to rotate the body about its vertical axis, supporting the generation of peak whole-body angular momentum near ball release, which is when our simulation terminated. Modelling the rear foot as remaining in contact with the ground until ball release therefore preserved the mechanism by which the rear leg contributes angular impulse to the trunk–arm complex, a pathway plausibly linked to ball velocity via transfer of angular momentum up the kinetic chain [35]. Enforcing rear-foot contact with the ground until ball release did not constrain post-release recovery mechanics, yet it ensured that the model could realize the rear-leg contribution to angular impulse that coaches often emphasize and that serves an important function in pitching [35]. These findings support the modelling decision to enforce contact between the rear foot and the ground with a point constraint from peak lead knee height to ball release. The original and revised models are shown in Fig. 1.

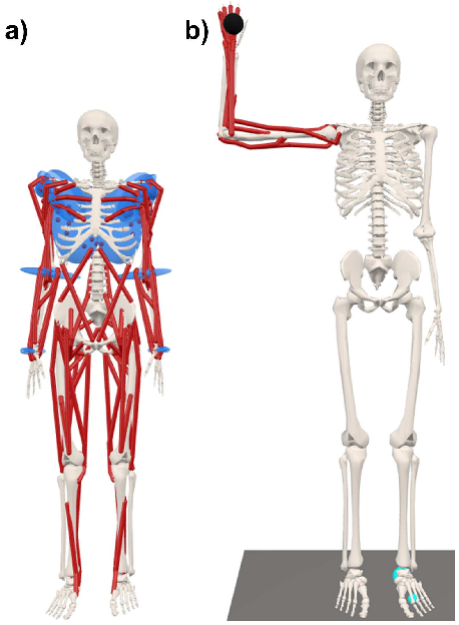

Fig. 1 (a) Base OpenSim musculoskeletal model developed by combining the models from Delp et al. and Holzbaur et al., and assembled by Andrea Menegolo [5, 9, 10, 17–20]. (b) Revised OpenSim musculoskeletal model for use in forward dynamic simulations of pitching. The revised model was scaled to the proportions of an MLB starting pitcher, includes a baseball, contains the 15 essential muscles for our study of UCL loads, and includes the ground. Ground contact was modelled with contact spheres (left foot) and a spherical joint (right foot). Developed in OpenSim.

2.2 Optimal Control of the Pitching Motion

Optimal control of the model was used to determine the pitching motion that minimized UCL loading while maintaining pitching speed. The OpenSim Moco software was used to solve the optimal control problem, which involved minimizing actuation effort while achieving a competitive pitch speed [36]. Constraints were imposed on joint angles and speeds, muscle activations, and ball speed to reflect realistic bounds for elite athletes. The final cost function of the optimal control problem rewarded reaching a desired pitch speed threshold, achieving a lead-foot speed of zero at ball release (to maintain balance and prevent slipping), and minimizing the actuation of the shoulder rotation reserve actuator in particular, which tends to further load the UCL [2, 7, 11]. All actuator outputs (muscles and reserve actuators) were minimized to reduce oscillations in the actuator controls that are products of the time discretization used by the Moco optimization [36]. Each muscle and reserve actuator was assigned a relatively low cost weight (0.001), with the exception of the shoulder rotation reserve actuator (1), given its contributions to UCL loading (see Section 2.3). The ultimate goal of the optimizer was to minimize actuation effort (with particular attention to the throwing shoulder rotation DOF), subject to endpoint constraints of zero lead-foot speed and achieving the desired ball speed at release.

Actuation effort represented the absolute values of torque (for reserve actuators) and force (for muscles) as a function of their control input, integrated over the motion duration. Controls were parameterized as piecewise linear functions of time that represented the amplitude of control signals (for reserve actuators) and excitations (for muscles). The controls vector sampled the value of reserve actuator controls/muscle excitations at 1 ms intervals, where the vector size was equal to the combined number of muscles (15) and actuators (34) in this model (49 total) times the number of time points. All simulations were of 1 s duration to maintain consistency in the number of states and controls in each iteration of the optimization. A duration of 1 s was sufficiently long to complete the throwing motion. Simulation results were truncated to retain only the pitching phases of interest, from peak lead knee height to ball release. The instant of ball release was identified as the frame corresponding to the maximum linear velocity of the throwing hand in the direction of home plate (the positive X-axis). The simulation results following ball release (which were often nonphysical) were ignored in subsequent analyses.

Cost functions and equality constraints were not defined directly in Moco's optimization framework. They were implemented using Moco's custom optimization functions, which can be tailored to different problems. Actuation minimization was achieved using the *MocoControlGoal*, where muscle and reserve actuator effort were specified, while *MocoFinalOutputGoal* was used to assign the endpoint constraints on foot and ball speed. *MocoFinalOutputGoal* provides functionality to assign weights to the endpoint constraints, which was done in this model to penalize deviations from the desired final values. Considering the weighted endpoint constraint terms as penalties (soft constraints), the cost function was as follows:

$$J = W_1 \left(\frac{v_{\text{ball, final}} - v_{\text{ball, desired}}}{v_{\text{ball, desired}}} \right)^2 + W_2 \left(\frac{v_{\text{foot, final}}}{v_{\text{foot, maximum}}} \right)^2$$

$$+ \sum_{i=1}^{n_{\text{actuators}}} C_i \left(\frac{\text{actuation effort}_i}{\text{maximum effort}_i} \right)^2 \tag{1}$$

subject to
$$|v_{\text{ball, final}} - v_{\text{ball, desired}}| \leq 0.0001 \text{ m/s}$$
$$|v_{\text{foot, final}}| \leq 0.0001 \text{ m/s}$$
$$-1 \leq \text{controls}_{\text{ actuators}} \leq 1$$
$$0 \leq \text{controls}_{\text{ muscles}} \leq 1$$

where $W_1 = 15, \quad W_2 = 5$

$$C_i = \begin{cases} 1, & \text{for the shoulder rotation actuator} \\ 0.001, & \text{otherwise} \end{cases} \qquad i = 1 \ldots n_{\text{actuators}}$$

The absolute magnitudes of the cost function weights were less important than their relative magnitudes (see Section 3.1). The hierarchy we used reflects the prioritization of a pitcher's performance when pitching, where the magnitudes were identified through trial and error. Each cost function term was squared to ensure that the terms were positive and the function was smooth and differentiable, which simplifies the search space and derivative calculations for the direct collocation optimal control method used in OpenSim Moco [36]. Additionally, the cost function terms were all normalized to ensure a unitless output.

A two-step optimization approach, commonly used in Moco-based optimal control, was employed to enhance robustness and ensure convergence [37]. The first step utilized a tracking optimal control simulation (*MocoTrackingGoal*) which used the mean joint angle trajectories from the inverse kinematic analyses extracted from Visual3D as input, and minimized the sum of squared errors between the experimental and simulated joint trajectories. The output of this simulation provided joint trajectories for each DOF in addition to the actuator controls and muscle excitations responsible for producing this motion, as was done by Buffi et al. [7]. This step provided a good initial guess for muscle excitations and joint angle trajectories, given that the excitations and joint angles were fit to an observed pitching motion. The second step minimized UCL load while maintaining the desired pitch speed, using the joint trajectory and control outputs of the first simulation as an initial guess. This two-step approach resulted in feasible pitching motions while addressing both performance and safety. This approach also ensured that the final solution was unique and did not simply track the kinematics of the initial guess.

2.3 Post-Processing and UCL Load Calculations

Simulation outputs included kinematic states (joint positions and speeds) and control inputs (muscle and actuator controls), along with joint and actuator forces and moments. To analyze UCL loading, post-processing followed Buffi et al.'s framework,

employing OpenSim's *Joint Reaction Analysis* to compute forces and moments responsible for maintaining elbow joint stability [7]. The analysis assumes that there is a force and moment balance at the varus–valgus centre of rotation of the elbow. In the force balance equation, the terms representing the varus–valgus contributions of the muscles are cancelled by relating the net moment imposed by the subject's motion to the counter-moments from the musculoskeletal anatomy, as described by Buffi et al. [7]. This approach identifies the contributors to valgus loading as the indirect valgus torque at the elbow due to the arm's inertia and shoulder rotation, while the key resistor to a valgus load was shown to be the osseous articulation (joint compression) moment [6, 7]. The compression force of the elbow joint was necessary to calculate the osseous articulation moment. This moment was found by isolating the component of the compression force vector aligned with the radius's longitudinal axis and orthogonal to the varus–valgus axis of the elbow. This component of the osseous articulation moment represents the compressive load experienced by the elbow joint over time and is denoted by $F_{\mathrm{JC}}(t)$. To calculate the UCL load, $M_{\mathrm{UCL}}(t)$, where $M_{\mathrm{UCL}}(t)$ is defined as the net elbow valgus moment being resisted by the UCL, a method following the work of Buffi et al. was implemented [7]:

$$M_{\mathrm{UCL}}(t) = T(t) - M_{\mathrm{Art}}(t) = T(t) - (F_{\mathrm{JC}}(t) \cdot d_{\mathrm{Art}}) \tag{2}$$

where $T(t)$ is a valgus torque–generating actuator that uses results from the predictive simulation (according to Buffi et al., this is a varus–valgus torque), and $M_{\mathrm{Art}}(t)$ is a valgus-resisting moment, known as the osseous articulation or joint compression moment. In the work of Buffi et al., d_{Art} was half the length of the vector from the joint centre to the medial edge of the elbow (radius), perpendicular to the varus–valgus axis of rotation, and functioned as a moment arm. Based on measurements in the scaled musculoskeletal model, d_{Art} was found to be 18.6 mm.

For each simulation, the joint compression force profile in the elbow and the corresponding UCL load were calculated. Equation (2) shows that the valgus load on the UCL is driven by torque from the reserve actuator at the varus–valgus DOF, $T(t)$, while the joint compression force provides an opposing varus moment for stability. The model of Buffi et al. included an additional varus–valgus DOF at the elbow, which appears as $T(t)$ in Eq. (2) [7]. Their decision to add an additional varus–valgus DOF at the elbow may not be physiologically justifiable, despite them restricting that DOF with no range of motion, as valgus loading at the medial elbow is an inertial byproduct of shoulder external rotation during pitching [1–3, 11, 38]. Instead, we attribute this torque to the shoulder rotation reserve actuator, which is more consistent with anatomy while maintaining the dynamic consistency of Eq. (2) [1, 3]. This adjustment shifts the rotational driver, $T(t)$, found in the throwing arm from the distal end of the humerus (elbow) to the proximal end (shoulder). Consistency is maintained given that the shoulder's axis of rotation remained parallel to the elbow's varus–valgus axis of rotation because of the definitions of the model's local joint coordinate systems. While the decision of Buffi et al. to add an additional varus–valgus DOF at the elbow with no range of motion is a valid approach, we have included in our calculation the physiologically justified contributions of shoulder rotation to valgus loading of the elbow

[1–3, 7, 11, 38]. As such, we set $T(t)$ to represent the shoulder rotation reserve actuator torque. A figure of the forces and torques considered when calculating the UCL loads is included in Appendix B.

Post-processing of the simulations extracted key metrics from the Moco output. Metrics of interest included inputs for the UCL loading equation, muscle forces, and actuator contributions to UCL torque. Additionally, joint states and reaction forces, particularly elbow compression forces, were analyzed to assess their role in resisting moments on the UCL. UCL loading patterns were visualized during the critical arm-cocking and acceleration pitching phases using Python. The study employed MATLAB algorithms and OpenSim tools to analyze UCL loading, focusing on shoulder rotation actuator control and elbow joint compression forces. The magnitude of shoulder rotation actuator torque was derived as a function of its control signal. The control values (ranging from -1 to 1) were multiplied by the maximum shoulder rotation torque of 450 N·m, which was determined from the inverse dynamic analyses in Visual3D.

2.4 Case Studies

Three case studies were evaluated to study the effects of the optimization process on the simulated motion: (1) a 93 MPH (41.6 m/s) pitch, (2) a 110 MPH (49.2 m/s) pitch, and (3) a pitch optimized to minimize valgus moment at the elbow [39]. Each simulation produced unique pitching techniques and kinematic variations, with Case 3 incorporating an additional cost function term for directly minimizing valgus moment, $M_{\mathrm{UCL}}(t)$, at the elbow. All case studies used the previously described optimization framework, with some noted adjustments. See Appendix C for a detailed description of the cost function and mathematical expression used in Case 3. We augmented the original cost function (Eq. (1)) with a term that directly penalizes the elbow's valgus joint-reaction moment, which corresponds to the load resisted by the UCL. This new cost function term was integrated over time so that the optimizer favoured solutions that reduced medial-elbow torque across the entire motion rather than at only one instant. In OpenSim Moco, this cost function term was implemented with a *MocoJointReactionGoal* targeting the elbow joint and the valgus component (about the negative Y-axis), expressed in the upper-arm (parent) frame.

In this work, UCL loading was computed in post-processing of simulations and was not part of the primary optimization objectives of Cases 1 and 2 (Eq. (1)). To explore the implications of considering this metric directly in the cost function, Case 3 included an additional term that penalized valgus torques throughout the motion (see Eq. (3) in Appendix C). While this additional cost function term reflects the trade-off between UCL load mitigation and performance, it also prevented the model from achieving competitive ball speeds (see Section 3), suggesting that directly minimizing UCL load can constrain the solution and prevent the kinetic-chain coordination required for high-velocity pitching. All cost functions penalized recruitment of the shoulder rotation reserve actuator (a proxy for UCL load; see Section 2.3), which preserved the performance–load balance by discouraging extreme valgus torques while allowing the optimizer to redistribute effort to attain target velocities. The inclusion, and subsequent results, of the additional UCL-load term in the cost function for Case 3

suggests that UCL loads and pitch speed are in direct competition. Although increasing the weight of the shoulder-rotation reserve actuator term may be analogous to the additional cost function term in Eq. (3), this additional term directly addressed the desired intent of the third case study, which was to explore the effect of directly minimizing valgus loads. Increasing the weight of the shoulder-rotation reserve actuator term penalized that input; the optimizer can evade that penalty by shifting effort to other joints or timings while still producing a similar valgus moment at the elbow. The extra term in Eq. (3) instead penalized the elbow's valgus load over the entire motion, and therefore could not be evaded by redistributing torques, passive forces, or interaction effects.

3 Results and Discussion

The first case study simulated a 93 MPH (41.6 m/s) pitch, the MLB average speed, by solving an optimization problem that constrained solutions to this threshold. The simulated motion, completed in 0.44 s, resembled traditional pitching mechanics, with some notable differences, but compared favourably with the inverse kinematics data (see Section 3.4). The optimized solution produced adjustments in trunk tilt and arm slot position that have been correlated with elevated UCL loads and increased ball speeds in the literature [40]. Notably, adopting kinematics with slight contralateral trunk tilt and an arm slot not aligned with the shoulder (Fig. 2a) produced a competitive pitch speed with expected UCL loads (Fig. 3) [7, 40]. However, the level of shoulder abduction was inconsistent with what one would expect from a competitive pitcher [40].

The second case study simulated a 110 MPH (49.2 m/s) pitch, exceeding the fastest in-game MLB pitch by 5 MPH [39]. The motion, completed in 0.47 s, prioritized ball speed but deviated from typical pitching mechanics, resembling a cricket bowl (Fig. 2b). Extreme contralateral trunk tilt and an overhead arm slot were observed, alongside destabilizing lower-body mechanics, such as crossed-over feet during the stance phase. Adopting these extreme kinematics produced greater loads on the UCL, aligning with the claims in the literature that an overhead arm slot and contralateral trunk tilt increase loads on the UCL (Fig. 3) [40]. However, the overhead arm slot observed was a result of the extreme contralateral trunk tilt instead of expected shoulder abduction.

The third case study introduced an additional term in the cost function that minimized valgus torque to directly reduce UCL load (in addition to the default minimization of shoulder rotation actuation), targeting a pitch speed of 93 MPH (41.6 m/s). However, the simulation failed to converge at 93 MPH and only succeeded at 75 MPH (33.5 m/s), producing a complete motion in 0.65 s. This pitch featured a sidearm slot, severe ipsilateral trunk tilt, and low shoulder rotation, characteristics of low UCL loads but also slow ball speed (Fig. 2c). The limited shoulder rotation observed when directly minimizing valgus loads at the elbow (Eq. (3)) demonstrates the effect of shoulder rotation on UCL load and supports its use in the UCL loading equation (Eq. (2)) as $T(t)$. Despite the only change in this simulation being the additional cost function term (to minimize elbow valgus torque directly), the results demonstrated the lowest shoulder external rotation range of motion and, ultimately,

the lowest overall UCL loads (Fig. 3). This result suggests that reducing shoulder external rotation may be correlated with reducing UCL loads, which would align with findings reported in the literature that attribute this shoulder external rotation to valgus load on the elbow [1–3, 11, 38]. These results may explain why MLB pitcher Tyler Rogers, who exhibits similar mechanics, has avoided UCL injuries with similar fastball velocities [39]. Historically, pitchers with low arm slots as exhibited in this simulation also have slower-than-average fastball speeds [39]. These pitchers often rely on deception and change of speeds rather than top-end pitch speeds, so the fact that this simulation failed to produce competitive speeds supports the idea that these mechanics limit speed generation.

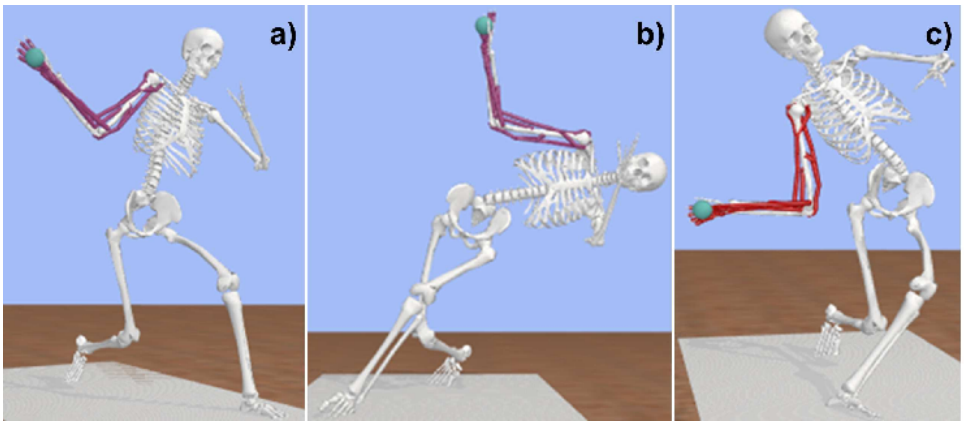

Fig. 2 Simulated pose of the forward dynamic model at ball release for the a) 93 MPH and b) 110 MPH pitches, and c) for the pitch that minimizes valgus torque at the elbow. Developed in OpenSim.

Comparisons between the case studies highlighted the trade-offs between performance and injury mitigation. The analysis of varus–valgus torque at the elbow provides insights into UCL loading as the simulated kinematics change across the case studies, particularly at ball release (Fig. 3). The muscle force profiles for all case studies are shown in Fig. 4.

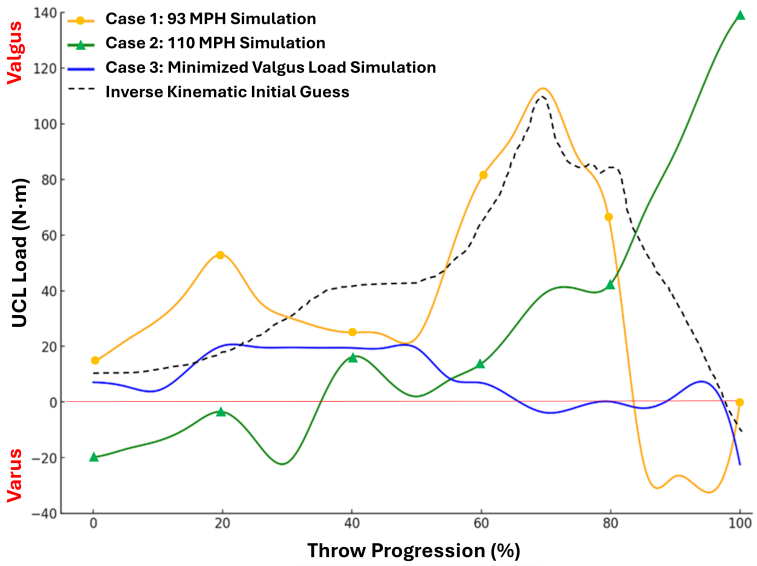

Fig. 3 UCL load for three case studies during arm-cocking and acceleration phases to release. 0% corresponds to initiation of arm-cocking; 100% represents the instant of ball release. Given that ligaments can bear only positive loads (tension), a negative torque indicates that the UCL is experiencing zero load. Developed in Python.

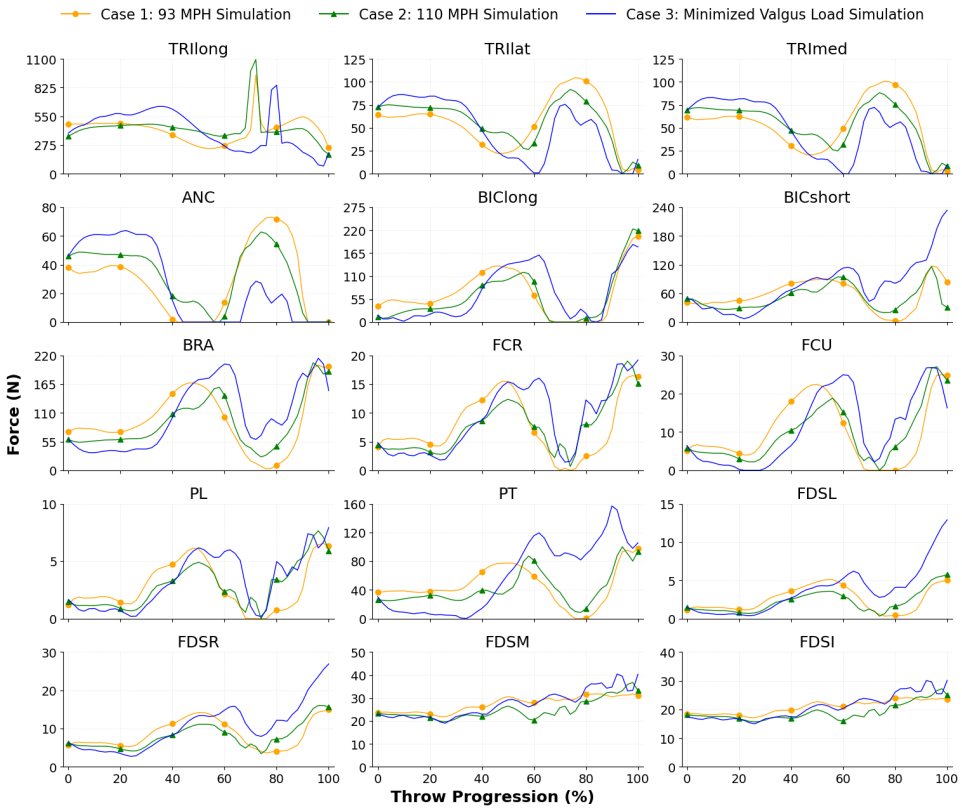

Fig. 4 Muscle forces across three case studies during arm-cocking and acceleration phases to release. 0% corresponds to initiation of arm-cocking; 100% represents the instant of ball release. 70% to 90% represents the arm acceleration phase. The muscle abbreviations are as follows: triceps (TRIlong, TRIlat, TRImed), anconeus (ANC), biceps (BIClong, BICshort), brachialis (BRA), flexor carpi radialis (FCR), flexor carpi ulnaris (FCU), palmaris longus (PL), pronator teres (PT), and the four flexor digitorum superficialis muscles (FDSL, FDSR, FDSM, FDSI). Developed in Python.

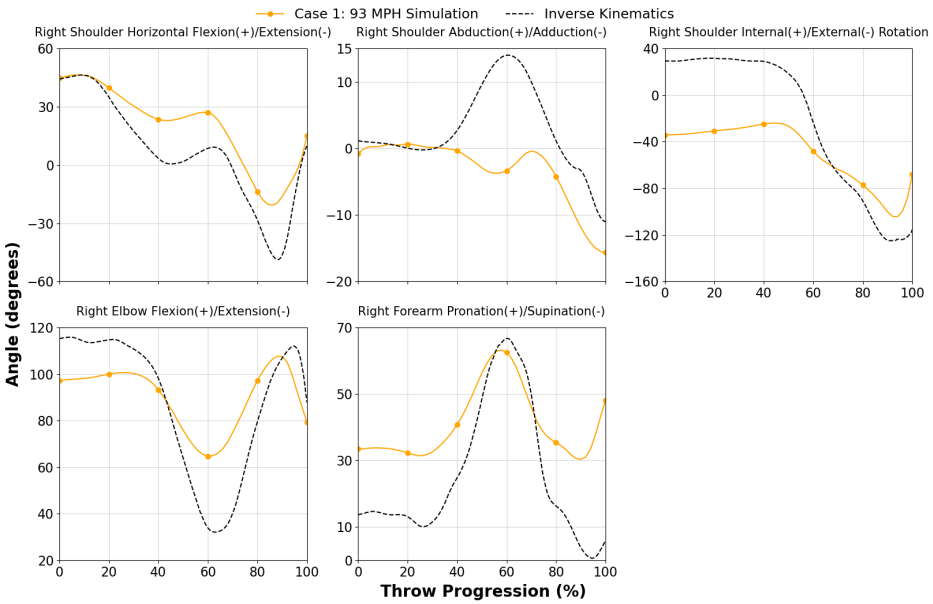

Fig. 5 Comparison of arm kinematics between experimental (Inverse Kinematics) and simulated (Case 1: 93 MPH Simulation) joint trajectories during arm-cocking/acceleration initiation (0%) to release (100%). Neutral position is defined as a T-pose with the palms facing downwards. Developed in Python.

3.1 Validation of Predictive Simulations

The model was validated by comparing to literature, performing sensitivity studies, and evaluating simulation consistency. Although direct experimental validation was constrained by a lack of comparable data, the simulation framework demonstrated robustness in producing plausible pitching motions.

The model's ability to estimate valgus loading and muscle coordination was assessed by comparing to findings from Buffi et al. [7] and Anz et al. [41]. Simulated peak UCL loads of 117 N·m (Case 1) were similar to the values reported in the literature, where Buffi et al. and Anz et al. reported loads of 115 N·m and 100 N·m, respectively. Furthermore, the UCL load profile from the inverse kinematic initial guess (Fig. 3) closely resembled the UCL load profile reported by Buffi et al. (both results relied on measured kinematics). Both the literature [7] and this work identified the three triceps compartments as primary contributors to elbow stabilization during peak valgus loading, based on their force profiles (Fig. 4). Furthermore, the inverse kinematic and experimental observations in Case 1 showed some similarities, but also some notable differences, specifically in shoulder abduction/adduction and rotation, which will be discussed in Section 3.4 (Fig. 5). However, discrepancies in the motion compared to Buffi et al. were noted in elbow flexion and forearm pronation trajectories, which may stem from differences in optimization methodologies and the scope of analysis. For example, Buffi et al. considered follow-through dynamics while the present model focused on pre-release phases. Moreover, differences in elbow flexion and pronation trajectories between this model and that of Buffi et al. may have occurred as a result of the absence of the varus–valgus DOF in our model, which was instead relocated to the shoulder in our model.

Sensitivity studies were conducted to assess the simulation framework's robustness. First, adjustments to initial guesses were considered, including kinematics from other pitchers and trials. Although the model was developed using data from a single pitcher (Pitcher 1), data from five pitchers were available. Mean joint angles from Pitchers 2 through 5, as well as ten randomly selected pitching trials for each pitcher, were selected as initial guesses for use in the sensitivity studies. The simulation of these initial guesses produced consistent within-pitcher results, reflecting the model's ability to adapt to natural variability in a single pitcher's motion. Specifically, the model consistently produced similar joint angles, quantified through root mean square error calculations on joint trajectories (which were always less than 5 degrees), and a similar total motion time for a given pitcher. Variability was observed between pitchers, particularly in arm slot and shoulder abduction, highlighting the influence of individualized kinematics on optimization outcomes. While these differences underscore inter-individual variability, all motions remained biomechanically plausible, as demonstrated through the observed ROM for all simulations, which remained within the anatomical boundaries [9].

Next, sensitivity to cost function weights in the optimization problem was studied. Arbitrary changes to the cost function weights (W_1, W_2, and C_i in Eq. (1)) were made, reflecting different orders of importance among the objectives. The sets of weights were chosen to disrupt the initial hierarchy and evaluate the model behaviour when foot speed or actuation effort were prioritized over ball speed. The implementation of these

simulations followed the procedure for Case 1. Simulations consistently converged to plausible motions when the weights prioritized ball speed over final foot speed with actuator torque weighted lowest (Table 1), which aligns with the procedure used in the case studies. Failures to converge occurred when deviations from this hierarchy were introduced. For example, prioritizing actuator torque minimization yielded insufficient pitching speed, while reducing the weight of the lead-foot final speed caused the model to slip and fall.

Table 1 Sensitivity Study Results While Varying Cost Function Weights ($C_i = 0.001$ for all other actuators in all cases).

Study	Ball Speed (W_1)	Foot Speed (W_2)	Shoulder Rotation Actuation Effort (C_i)	Outcome
1	15	5	1	Baseline
2	8	10	15	Failed
3	10	15	2	Failed
4	15	5	3	Converged
5	15	5	10	Failed
6	15	7	1	Converged
7	15	10	2	Converged
8	17	7	1	Converged
9	18	4	2	Converged
10	18	6	1	Converged
11	20	5	1	Converged
12	20	8	2	Converged
13	22	6	2	Converged
14	25	7	3	Converged
15	30	10	1	Converged

In each study that converged, similar outcomes were achieved with respect to the baseline simulation, reaching the desired ball speed outlined in Case 1/Study 1 (93 MPH), in addition to producing consistent joint angles (as quantified by Study 1). Three unique failure modes were observed when the hierarchy of cost function terms was disrupted. In Study 5, where the actuation effort weight exceeded the final foot speed weight, the simulation failed due to the front foot slipping. In Study 3, prioritizing lead-foot final speed over ball speed resulted in decreased ROM in all joints of the lower body, which may have led to the observed decrease in ball speed that prevented convergence [42]. Moreover, in Study 2, prioritizing actuation effort minimization led to insufficient shoulder rotation ROM, resulting in slow ball speed and subsequent failures to converge. These findings align with the biomechanics of real-life pitching scenarios, where performance (i.e. maximizing ball speed and lead-foot stability/balance) is prioritized over conscious injury mitigation (i.e. minimizing UCL load). In future studies, a more detailed analysis of the converged cases noted in Table 1 is warranted to determine the extent to which the simulation results reflect the expected outcomes when changing cost function weights.

Further examination was conducted to assess the plausibility of the simulated GRFs. Specifically, we examined the 3D force vectors generated by the lead-foot heel contact sphere and the reaction forces at the rear-foot point constraint, resolved along the vertical, anterior–posterior, and medial–lateral axes. The examination was conducted for Case 1, as this simulation represented the most traditional pitching motion. These results are presented in Fig. E3 and Fig. E4, respectively, in Appendix E. We

are unaware of publications reporting GRFs in professional pitchers; existing studies have focused on amateur populations. Comparison to an amateur population is imprudent as professionals typically produce higher ball speeds and have greater body mass, likely yielding greater GRFs than those reported in the literature for amateur pitchers. As such, we have restricted our analysis to observations of the GRF profiles.

First, the vertical GRF remains positive for both feet, confirming that the ground never pulls the feet downward in the simulation. Second, the trajectories of all GRF components exhibit the expected qualitative patterns for both feet. The lead-foot heel contact force (Fig. E3) remained zero until approximately 87.3% of the throwing progression. Upon initial contact, the vertical heel force exhibited a brief but large spike exceeding 2× body weight (BW), which then decreased to zero as the forefoot contact sphere applied a substantial posterior force (nearly 2× BW). These large GRF magnitudes are consistent with the impulse required to transfer lower-body momentum up the kinetic chain to the arm. The spherical joint reaction vertical forces (Fig. E4) also exhibited expected behaviours. The vertical force began near 1.0× BW at 0% throw progression (single support on the rear foot), increased to a peak of approximately 1.4× BW as the knees and hips flexed, and then decreased as the model's weight shifted forward and the rear foot unloaded approaching ball release. The presence of anterior and lateral components of the rear-foot GRF reflects the typical demands of propulsion and balance that drive the centre of mass toward the batter. The lateral component of the GRF decreased to zero as the rear foot pivoted. Vertical and posterior components of the GRF near ball release reflect the spherical joint enforcing toe-to-ground contact through the prevention of translation. While these findings are encouraging and consistent with expected mechanics of professional baseball pitching, the lack of comparable experimental GRF data remains a limitation. Future work will include collection of force-plate GRFs to quantitatively validate the simulated forces.

Our results are consistent with literature, consistent across simulations with different inputs, and adaptable to varying initial conditions and cost function weights, collectively providing confidence in our simulation framework in analyzing MLB pitches [6, 7, 41]. While some discrepancies were observed, particularly in inter-individual variability, the results demonstrate the simulation framework's robustness and reliability in replicating key aspects of pitching motions. Moreover, the differences observed between the simulated UCL load of the initial guess simulation and the three case studies (Fig. 3) are due to the optimization framework's ability to produce unique motions, not merely tracking kinematic inputs. Despite these differences, the subtle similarities across simulations, experimental data, and literature demonstrate the ability of the forward dynamics approach to produce plausible novel kinematics in a unique pitching motion.

3.2 UCL Loading

Case 1 (93 MPH) simulated a traditional pitching motion (Fig. 2a) and torque profile (Fig. 3), showing a peak valgus torque of approximately 117 N·m, which was consistent with values observed in literature (see Section 3.1) [7, 41]. However, early motion phases in Case 1 deviated from Buffi et al.'s arm kinematics, which may have stemmed from actuation minimization in the arm, potentially yielding more subtle movements

in shoulder abduction and elbow flexion. Despite these early-phase differences, the critical late phases (e.g., the instant of maximum external shoulder rotation, where the peak UCL load was observed) show similarities in UCL loading patterns.

Case 2 (110 MPH) exhibited the highest valgus torque (140 N·m) and an atypical torque profile (Fig. 3), driven by extreme contralateral trunk tilt and an overhead arm slot (Fig. 2b). These kinematic adjustments suggest that extreme contralateral tilt impacts valgus torque by increasing the moment arm and mechanical demand on the elbow, supporting the findings of Hakanson et al. [43].

Case 3 (75 MPH), designed to minimize valgus torque, reduced peak UCL load to 20 N·m (Fig. 3) through extreme sidearm delivery and ipsilateral trunk tilt (Fig. 2c). These adjustments shortened the valgus moment arm and reduced shoulder external rotation, kinematic patterns that are consistent with reduced UCL loads [2, 3, 11, 38, 43]. However, these changes reduced ball speed, demonstrating a trade-off between performance and injury prevention.

Case 3 exhibited loads that were greater in magnitude than those for Case 1 near the end of the throw progression (ball release), which seems to contradict the optimization objective (i.e. we would expect Case 3 to produce the smallest UCL loads). This discrepancy is a result of the optimizer in Case 3 aiming to reduce valgus torque during the power-generation (arm-cocking and acceleration) part of the throw, not aiming to minimize the absolute elbow moment across the entire motion. As a result, the large mid-throw valgus peak was avoided but a greater late-phase moment was permitted that was mostly varus, which did not strain the UCL and therefore was not strongly penalized in the cost function (particularly the term responsible for the actuation of shoulder rotation). The cost function for Case 3 (see Appendix C) also penalized large values of *valgus* torque on the elbow whenever they occurred, not just at one instant. As such, this additional term could lead to increased torques at some instances compared to Case 1, but overall, the valgus torque magnitude was substantially lower than in Case 1.

Further simulations examining pitches with ball speed between 75 and 110 MPH revealed an approximately linear increase in valgus torque as ball speed increased, with a shallower slope beyond 93 MPH (Fig. 6). This result suggests that UCL loading does not increase proportionally with higher ball speeds. The results shown in Fig. 6 provide insight into the biomechanical demands of pitching, suggesting a trade-off between ball speed and injury risk, offering a basis for future explorations of performance optimization and injury prevention in baseball pitching.

3.3 Muscle Behaviours

The muscle activations in the 93 MPH simulation highlighted critical phases of the pitching motion (Table 2). Muscle activations peaked during the arm acceleration phase (70% to 90%), with the three triceps compartments exceeding activation levels of 0.8. These muscles may be key contributors to rapid elbow extension, crucial for generating high velocity at the elbow, as evident by the steep onset of peak activation of the triceps observed during the arm acceleration phase. This result supports the findings of Acosta et al. [44], who showed that the three triceps compartments are

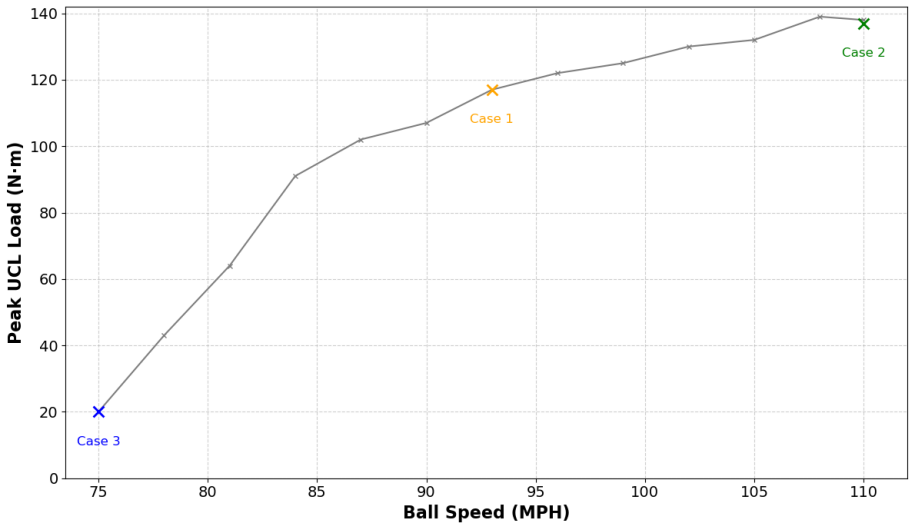

Fig. 6 Peak UCL load vs. ball speed for the three case studies and additional simulations. Case 1: a 93 MPH (41.6 m/s) pitch, Case 2: a 110 MPH (49.2 m/s) pitch, and Case 3: a pitch optimized to minimize valgus moment at the elbow. Developed in Python.

the largest contributors to elbow extension velocity during pitching, and strengthening these muscles leads to increased pitching performance. Furthermore, a study by McCutcheon et al. [45] showed that pitchers with higher ball speeds also demonstrated greater elbow extension velocities. The PT, BRA, and biceps also exhibited high activations, with PT peaking at 0.73 and BRA at 0.68, supporting previous findings that these muscles are important for stabilizing the forearm and protecting the elbow during pitching [7, 46]. The FCR and FCU showed moderate peak activations (0.5–0.6), supporting existing studies that identify their role in counteracting valgus forces and stabilizing the medial elbow [46]. Finally, both heads of the biceps showed spikes in activation during the arm acceleration phase, suggesting their importance in resisting the rapid elbow extension during pitches.

Table 2: Peak Muscle Activation During Arm Acceleration and Corresponding Throw Progression for the 93 MPH Simulation

Muscle	**Peak Activation (% Maximum)**	**Throw Progression at Peak (%)**
Anconeus (ANC)	57	90
Biceps Brachii Long Head (BIClong)	58	71
Biceps Brachii Short Head (BICshort)	59	82
Brachialis (BRA)	68	81
Flexor Carpi Radialis (FCR)	58	71
Flexor Carpi Ulnaris (FCU)	55	80
Flexor Digitorum Superficialis Index (FDSI)	58	72
Flexor Digitorum Superficialis Long (FDSL)	51	87
Flexor Digitorum Superficialis Middle (FDSM)	60	72
Flexor Digitorum Superficialis Ring (FDSR)	53	72
Palmaris Longus (PL)	53	79
Pronator Teres (PT)	73	82
Triceps Brachii Lateral Head (TRIlat)	81	83
Triceps Brachii Long Head (TRIlong)	92	73
Triceps Brachii Medial Head (TRImed)	80	84

Comparisons of muscle forces (Fig. 4) across the three case studies reveal consistent patterns in timing and magnitude, with the triceps (TRIlong, TRIlat, and TRImed) consistently generating the greatest forces during the arm acceleration phase (70% to 90%). The valgus torque minimization case showed lower overall muscle forces, reflecting reduced valgus load, while flexor–pronator muscles (e.g., FCU, FCR, and PT) exhibited greater forces during acceleration, aiding elbow stabilization and counteracting valgus torque. Despite differences in pitching speed and kinematics, muscle force trajectories were similar across case studies. The triceps compartments and flexor–pronator group consistently peaked during arm acceleration, suggesting their importance in elbow stabilization and dynamic protection [46].

Differences in ball speed between the three case studies may be attributed to differences in the kinematic contributions of the trunk, pelvis, and lower extremities, given the similarity of muscle force production across case studies. In the optimized throwing motion of Case 1, the trajectory of the arm relative to the thorax appears similar to the initial inverse-kinematic guess despite differences in full-body mechanics (see Fig. 5). For example, the 110 MPH simulation (Case 2) exhibited exaggerated contralateral trunk tilt and greater angular velocity of the throwing arm than Cases 1 and 3, increasing ball speed but altering arm kinematics and dynamic demands on the elbow. In contrast, the valgus-torque minimization case (Case 3) used a sidearm motion with ipsilateral trunk tilt, reducing muscle forces yet maintaining consistent muscle-force patterns. Differences in the magnitudes of throwing-arm joint angles between Case 1 and the initial inverse-kinematic guess were observed. Comparisons to Cases 2 and 3 were not possible due to the novelty of these motions and a lack of experimental data in the literature. Despite the magnitude differences in Case 1 and the inverse kinematic simulation, the kinematic trajectories exhibited similar patterns over time, suggesting that the underlying arm path relative to the thorax was conserved. The similarity of temporal patterns in arm kinematics despite differences in ball speed is consistent with the view that whole-body mechanics proximal to the arm can modulate ball release speed [42]. These findings underscore the interconnected nature of the pitching motion, in which deviations in trunk–pelvis–lower-limb mechanics affect elbow loads even when arm-trajectory patterns remain relatively consistent (Fig. 5) [42]. The ability to maintain arm paths across different ball speeds and full-body mechanics, despite changes along the kinetic chain, underscores the importance of integrated full-body optimization in analyses of pitching strategies [47]. Future studies should explicitly quantify trunk–pelvis–lower-limb contributions to ball speed while controlling for arm-path similarity.

Results of the muscle behaviour analysis align with the study by Seiber et al. [46], which highlighted the stabilizing role of the triceps, biceps, and brachialis in reducing varus–valgus laxity during dynamic elbow motion. Furthermore, comparisons to the results of Buffi et al. [7] revealed similarities in muscle behaviour, where the triceps, biceps, and flexor–pronator groups demonstrated similar activation peaks and patterns during arm acceleration. Both studies identified the triceps compartments as primary contributors to the net varus moment at the elbow during peak valgus loading. This agreement demonstrates the biomechanical advantages of eccentric contractions during elbow flexion, which enable the triceps to generate high forces [26].

Furthermore, the dynamic interplay between the biceps and flexor–pronator groups, acting synergistically to protect the UCL, was consistent across the results of Buffi et al. [7], van der Pijl [6], and our model.

Reserve actuators are joint torques that are generated to represent moments produced by unmodelled structures and when the Hill-type muscle models cannot supply sufficient force at a given instant. Reserve actuators are expected to remain small (less than 10% of the peak joint torque) in a dynamically well-posed solution [27]. In our simulations, reserve activations were generally low and stable through the early- and mid-throw phases, with values typically within ±10% of the respective peak joint moment over the entire motion (see Appendix F). Brief excursions beyond this threshold were generally observed near ball release (approx. 90–100% of progression) for a subset of DOFs (i.e. shoulder horizontal flexion/extension and abduction/adduction, and wrist deviation), including brief negative excursions (greater than 10% of absolute peak joint torque). Namely, the reserve actuator torque for shoulder horizontal flexion for Cases 1 and 3 peaked at around 12 and 14% of peak joint torque; the reserve actuator torque for shoulder abduction for Cases 1, 2 and 3 peaked at around 25, 12 and 13% of peak joint torque; and the reserve actuator torque for wrist radial deviation for Cases 1, 2 and 3 peaked at around -22, 13 and -11% of peak joint torque, respectively. These spikes indicate instants when the modelled actuators approached their functional limits and the solver compensated with reserve actuators to satisfy the dynamic constraints. We therefore note as a limitation that muscle strength, muscle coordination, and/or controller fidelity near release may be insufficient to capture the rapid transients of late-phase throwing without assistance from reserve actuators. However, given that the peak reserve actuator activations were generally within recommended bounds, and excursions from these bounds were very brief within rapid phases of the pitching motion, the reserve actuators did not substantially affect the contributions of the muscles. Future work will focus on reducing these late-phase reserve actuator torques by refining muscle parameterization, adjusting controller structure and tracking weights, and exploring targeted model updates (e.g., joint stiffness/damping and musculotendon properties) so that the reserves remain within the recommended bounds throughout the motion.

3.4 Simulated Kinematics

Comparison of simulated pitching kinematics revealed unique characteristics across the three case studies, emphasizing the optimizer's ability to generate solutions independently of input kinematics. Case 1 (93 MPH), which had plausible kinematics, was compared against the inverse kinematics data from motion capture and literature, since it most closely resembled the inverse kinematics solution (i.e. a traditional pitch). While joint trajectories for shoulder horizontal flexion/extension, elbow flexion/extension, and forearm pronation/supination were within plausible ROM, differences in magnitudes between experimental and simulated data were observed (Fig. 5). For example, the optimized Case 1 pitch simulation predicted lower elbow flexion during the late cocking phase and less angular displacement in forearm pronation. These discrepancies likely reflect the optimizer's minimization of actuation (C_i in Eq. (1)). Furthermore, notable differences were identified in the degree of elbow extension during

the dynamic phases of the motion (Fig. 5). Rapid elbow extension is a key contributor to ball speed but also increases UCL loads, as supported by McCutcheon et al.'s study where they identified that faster pitchers consistently produced greater elbow extension velocity and greater UCL loads [45]. The differences in elbow extension at ball release may stem from minimization of joint actuation, but also potentially from the bound on elbow angular velocity, which was set to 3000 deg/s in our model. Fleisig [14] cites elbow extension angular velocities up to 2400 deg/s in collegiate pitchers, which are likely greater in an MLB population. Despite never reaching the bound on elbow extension angular velocity, the optimizer was still able to achieve competitive ball speeds, which may be attributed to contributions from the trunk and shoulder. If true, the optimizer's ability to consistently achieve desired ball speeds suggests that pitchers can pitch competitively without the need for the elbow extension velocities that tend to increase loads on the UCL, through the adoption of altered trunk and shoulder mechanics. However, while the adoption of minimal shoulder abduction at ball release (seen in all simulated Cases) may have some benefits on reducing UCL load, it may increase the risk of injury elsewhere, such as the shoulders, which is also common and punishing to a pitcher's career [2, 14].

Notable differences in joint angle magnitudes were observed in shoulder abduction/adduction, where the optimized motion maintained a relatively static abduction angle, diverging from the trajectory observed in the inverse kinematic data. This difference may be a result of the optimizer's emphasis on minimizing full-body actuation (C_i in Eq. (2)), which can reduce the observed ROM if actuation of that joint does not contribute to the optimization goal. Given that shoulder abduction/adduction actuation remained relatively constant (around 0.5), the minimized actuation primarily functioned to keep the arm statically abducted.

Furthermore, differences in the internal/external rotation of the shoulder were observed between the inverse kinematic and optimized (Case 1) motions (Fig. 5). In particular, shoulder rotation was positive at the beginning of the simulation in the inverse kinematics but negative in Case 1, resulting in very different initial postures. Despite the simulated motion of Case 1 having the inverse kinematics as an initial guess (internally rotated by approximately 40°), the shoulder in the solution for Case 1 was externally rotated by approximately 40°. These differences are likely a consequence of the optimizer's emphasis on minimizing shoulder-rotation actuation. Because the model trades kinematic similarity for lower control effort under dynamic constraints, the solution can move away from the inverse-kinematics initial guess and settle on a posture that reduces the shoulder-rotation actuation. In the upper limb, several joint configurations can achieve similar hand paths and release conditions; the optimizer seeks the configuration that minimizes the shoulder-rotation actuation.

Comparison of kinematics between Buffi et al. [7] and Case 1 revealed both similarities and differences. Both studies captured consistent patterns in shoulder internal/external rotation and shoulder horizontal flexion/extension, validating the simulation's ability to model shoulder dynamics during arm-cocking and acceleration phases. However, discrepancies in elbow flexion and forearm pronation were noted. For instance, Buffi et al. reported a sharper decrease in elbow flexion during acceleration compared to the smoother transition predicted by our optimizations. These differences

likely stem from differences in modelling assumptions and optimization methodologies. The comparison of our optimization results with inverse kinematic data and the results of Buffi et al. [7] underscores the strengths and limitations of our results. While the agreement in shoulder dynamics validates the simulation's plausibility in achieving the observed mechanics in a pitcher, the discrepancies in elbow and forearm kinematics reveal areas for refinement, such as the addition of elbow and wrist joint coupling constraints.

4 Conclusion

This study offers a novel approach to understanding and optimizing the mechanics of baseball pitching, with a focus on minimizing the risk of UCL injuries while maintaining or enhancing performance. This study is the first predictive dynamic simulation of baseball pitching: we adopt a two-step approach that does not strictly track input kinematics and estimate muscle activations based on observed motions, as was done in previous studies [6, 7, 10]. The optimizer's ability to produce novel motions is evident from the unique simulation outputs of Cases 2 and 3, and further emphasized by the differences in kinematics compared to experimental measurements and results reported in the literature.

Simulation results highlighted the strategies pitchers likely use to achieve competitive pitch velocities. The model demonstrated that aggressive mechanics, such as increased shoulder external rotation and excessive trunk tilt, can be effective at generating greater ball velocities, but they may also increase UCL loads. The analysis suggests the potentially critical role of the shoulder and elbow musculature, specifically the triceps and flexor–pronator group, in counteracting valgus torque during high-stress phases like arm-cocking and acceleration. The results emphasize the importance of incorporating full-body dynamics and standardized musculoskeletal modelling methodologies to capture the complex interplay between pitching mechanics and injury risk. Furthermore, Case 3, which specifically aimed to minimize valgus torque, demonstrated the direct trade-off between minimizing UCL loads and maintaining competitive pitch speeds, suggesting that valgus torques may be necessary for elevated ball speeds.

Future efforts should incorporate broader datasets and refine cost functions to enhance generalizability and reduce sensitivity to initial conditions. These improvements would strengthen the model's utility as a tool for understanding performance and injury mechanisms in baseball pitching. Moreover, while the forward dynamics model offers insights into pitching biomechanics, it has several limitations. The lack of directly comparable datasets or computational studies poses challenges for validation, particularly when novel pitching motions are simulated (Cases 2 and 3). While the reserve actuator activations (presented in Appendix F) are generally within the bounds suggested in literature [27, 48], there are some instances, particularly near ball release, where these bounds are violated. Future work will focus on reducing these late-phase reserve activations so that reserves remain within the recommended bounds throughout the motion. Furthermore, a key limitation of this work is the absence of synchronized experimental EMG data. Without EMG, we cannot directly

validate the timing, magnitude, or activation patterns of simulated muscle activations—particularly in late-cocking through ball release, when rapid torque transients occur and reserve actuators occasionally provided assistance. Access to high-quality surface or intramuscular EMG would enable stronger validation of the simulated motions. To our knowledge, no studies present experimental EMG data for professional baseball pitchers. Future studies will prioritize collecting synchronized EMG to perform activation-level comparisons and EMG-informed parameter tuning, thereby strengthening the physiological fidelity of the model and its conclusions. Assumptions about the contributions of the flexor digitorum superficialis (FDS) compartments to joint moments were also made and, while biomechanically plausible, also require experimental validation [7]. The model's reliance on anatomical parameters from multiple sources introduces potential biases, as noted in prior studies, and the omission of the scapular motion relative to the thorax limits the accuracy of shoulder dynamics [49]. Moreover, the use of more contact spheres on the lead foot would improve model accuracy, as it is difficult to encapsulate 3D GRFs using only two contact spheres. Future work should strive to use experimentally collected force-plate GRF data to validate the assumptions associated with using a spherical joint for the rear-foot contact and only two contact spheres for the lead foot. Future studies should also aim to quantify contributions to ball speed from the pelvis, trunk, and lower extremities, to show that variations in ball speed are impacted by kinematics outside of the throwing arm. Finally, the use of mean inverse kinematic joint trajectories to inform the design of the model's DOF and scaling the anthropometry to a single pitcher may reduce the model's generalizability across diverse sample populations.

In summary, the results of this study bridge gaps in the understanding of pitching biomechanics. We present a validated framework for simulating and optimizing pitching motions, emphasizing the importance of balancing performance objectives with injury prevention. The findings hold significant implications for personalized training programs, biomechanical interventions, and the development of advanced tools for real-time assessment of pitching mechanics.

Statements and Declarations

Contributions and Competing Interests

All authors contributed to the study conception and design. The research was led by Cedric E. Attias as part of a Master's thesis in Mechanical Engineering at the University of Waterloo. The first draft of the manuscript was written by Cedric E. Attias and all authors worked on previous versions of the manuscript. All authors read and approved the final manuscript. At the time of submission, Keaton Inkol and Cedric E. Attias are employed by the Seattle Mariners MLB organization. Thomas K. Uchida and John McPhee have no competing interests.

Ethics

Confidential athlete information is protected by a mutual non-disclosure agreement between the University of Waterloo and the MLB, and ethics approval was received

from the University of Waterloo to use and publish externally collected data. All parties involved provided written consent for the publication of this work.

Data Availability

Due to the confidentiality agreement between the University of Waterloo and the MLB, the data will not be made public. This includes the raw motion capture data from the MLB organization that was shared and anonymized by KinaTrax, and the OpenSim musculoskeletal model. This also protects athlete privacy, as outlined by the MLB's collective bargaining agreement between the league and its athletes.

Funding Statement

Financial support from the Canadian Institutes of Health Research–Canadian Graduate Scholarship: Masters, the Queen Elizabeth II Graduate Scholarship in Science and Technology, the Canada Research Chairs program, and the University of Waterloo is gratefully acknowledged. All funding was provided to Cedric E. Attias.

References

[1] Van Trigt, B., Vliegen, L.W., Leenen, T.A., Veeger, D.H.: The ulnar collateral ligament loading paradox between in-vitro and in-vivo studies on baseball pitching (narrative review). Int. Biomech. **8**(1), 19–29 (2021) https://doi.org/10.1080/23335432.2021.1916405

[2] Aguinaldo, A.L., Chambers, H.: Correlation of throwing mechanics with elbow valgus load in adult baseball pitchers. Am. J. Sports Med. **37**(10), 2043–2048 (2009) https://doi.org/10.1177/0363546509336721

[3] Calabrese, G.J.: Pitching mechanics, revisited. Int. J. Sports Phys. Ther. **8**(5), 652–660 (2013)

[4] Melugin, H.P., Leafblad, N.D., Camp, C.L., Conte, S.: Injury prevention in baseball: from youth to the pros. Curr. Rev. Musculoskelet. Med. **11**(1), 26–34 (2018) https://doi.org/10.1007/s12178-018-9456-5

[5] Delp, S.L., Anderson, F.C., Arnold, A.S., Loan, P., Habib, A., John, C.T., Guendelman, E., Thelen, D.G.: OpenSim: Open-source software to create and analyze dynamic simulations of movement. IEEE Trans. Biomed. Eng. **54**(11), 1940–1950 (2007) https://doi.org/10.1109/tbme.2007.901024

[6] van der Pijl, L.D.: Identification of muscles (un)loading the UCL during baseball pitching. Master's thesis, Delft University of Technology, Delft, Netherlands (2022)

[7] Buffi, J.H., Werner, K., Kepple, T., Murray, W.M.: Computing muscle, ligament, and osseous contributions to the elbow varus moment during baseball pitching. Ann. Biomed. Eng. **43**(2), 404–415 (2015) https://doi.org/10.1007/s10439-014-1144-z

[8] Gupta, D., Donnelly, C.J., Jensen, J.L., Reinbolt, J.A.: Goal-oriented optimization of dynamic simulations to find a balance between performance enhancement and injury prevention during volleyball spiking. Life **11**(7), 598 (2021) https://doi.org/10.3390/life11070598

[9] Xuan, B.E.W., Chan, S.S., Johan, H., Lim, L.S., Zuo, B., Ang, W.T.: Investigation of modeling differences between OpenSim and Visual3D for gait analysis of healthy gait. Proc. 16th Int. Conv. Rehabil. Eng. Assist. Tech., 42–46 (2023) https://doi.org/10.1145/3628228.3628492

[10] Anderson, F.C., Pandy, M.G.: Dynamic optimization of human walking. J. Biomech. Eng. **123**(5), 381–390 (2001) https://doi.org/10.1115/1.1392310

[11] Feltner, M.E.: Three-dimensional interactions in a two-segment kinetic chain. Part II: Application to the throwing arm in baseball pitching. J. Appl. Biomech.

5(4), 420–450 (1989) https://doi.org/10.1123/ijsb.5.4.420

[12] Chalmers, P.N., Erickson, B.J., Ball, B., Romeo, A.A., Verma, N.N.: Fastball pitch velocity helps predict ulnar collateral ligament reconstruction in Major League Baseball pitchers. Am. J. Sports Med. **44**(8), 2130–2135 (2016) https://doi.org/10.1177/0363546516634305

[13] Leland, D.P., Conte, S., Flynn, N., Conte, N., Crenshaw, K., Wilk, K.E., Camp, C.L.: Prevalence of medial ulnar collateral ligament surgery in 6135 current professional baseball players: A 2018 update. Orthop. J. Sports Med. **7**(9), 2325967119871442 (2019) https://doi.org/10.1177/2325967119871442

[14] Fleisig, G.: Biomechanics of baseball pitching: Implications for injury and performance. In: Proc. 28th Int. Conf. Biomech. Sports, Marquette, MI, USA, July 19–23, pp. 46–50 (2010)

[15] HAS-Motion, Inc.: Visual3D Documentation: OpenSim Kinematics and Kinetics. https://wiki.has-motion.com/doku.php?id=visual3d:documentation:kinematics_and_kinetics:opensim. Accessed: 2025-09-24 (2025)

[16] Uhlrich, S.D., Uchida, T.K., Lee, M.R., Delp, S.L.: Ten steps to becoming a musculoskeletal simulation expert: A half-century of progress and outlook for the future. J. Biomech. **154**, 111623 (2023) https://doi.org/10.1016/j.jbiomech.2023.111623

[17] Delp, S.L., Loan, J.P., Hoy, M.G., Zajac, F.E., Topp, E.L., Rosen, J.M.: An interactive graphics-based model of the lower extremity to study orthopaedic surgical procedures. IEEE Trans. Biomed. Eng. **37**(8), 757–767 (1990) https://doi.org/10.1109/10.102791

[18] Holzbaur, K.R.S., Murray, W.M., Delp, S.L.: A model of the upper extremity for simulating musculoskeletal surgery and analyzing neuromuscular control. Ann. Biomed. Eng. **33**(6), 829–840 (2005) https://doi.org/10.1007/s10439-005-3320-7

[19] Yamaguchi, G.T., Zajac, F.E.: A planar model of the knee joint to characterize the knee extensor mechanism. J. Biomech. **22**(1), 1–10 (1989) https://doi.org/10.1016/0021-9290(89)90179-6

[20] Anderson, F.C., Pandy, M.G.: A dynamic optimization solution for vertical jumping in three dimensions. Comput. Method. Biomech. Biomed. Eng. **2**(3), 201–231 (1999) https://doi.org/10.1080/10255849908907988

[21] Dillman, C.I., Fleisig, G.S., Andrews, J.R.: Biomechanics of pitching with emphasis upon shoulder kinematics. J. Orthop. Sports Phys. Ther. **18**(2), 402–408 (1993)

[22] Attias, C.: Dynamic modelling and simulation of Major League Baseball pitching

biomechanics to reduce ulnar collateral ligament injury and improve performance. Master's thesis, University of Waterloo, Waterloo, Canada (2025)

[23] Yanai, T., Onuma, K., Crotin, R.L., Monda, D.: A novel method intersecting three-dimensional motion capture and medial elbow strength dynamometry to assess elbow injury risk in baseball pitchers. Sci. Rep. **13**(1), 12253 (2023) https://doi.org/10.1038/s41598-023-39504-9

[24] Dempster, W.T., Gaughran, G.R.L.: Properties of body segments based on size and weight. Am. J. Anat. **120**(1), 33–54 (1967) https://doi.org/10.1002/aja.1001200104

[25] Wilk, K.E., Arrigo, C.A., Bagwell, M.S., Rothermich, M.A., Dugas, J.R.: Repair of the ulnar collateral ligament of the elbow: Rehabilitation following internal brace surgery. J. Orthop. Sports Phys. Ther. **49**(4), 253–261 (2019) https://doi.org/10.2519/jospt.2019.8215

[26] Millard, M., Uchida, T., Seth, A., Delp, S.L.: Flexing computational muscle: Modeling and simulation of musculotendon dynamics. J. Biomech. Eng. **135**(2), 021005 (2013) https://doi.org/10.1115/1.4023390

[27] OpenSim Documentation: Reserves and Residuals. https://opensimconfluence.atlassian.net/wiki/spaces/OpenSim/pages/53114407/_reserves+and+residuals. Accessed: 2025-09-24 (2015)

[28] Hortobágyi, T., Katch, F.I.: Eccentric and concentric torque–velocity relationships during arm flexion and extension—influence of strength level. Eur. J. Appl. Physiol. **60**, 395–401 (1990) https://doi.org/10.1007/BF00713506

[29] Cazzola, D., Holsgrove, T.P., Preatoni, E., Gill, H.S., Trewartha, G.: Cervical spine injuries: A whole-body musculoskeletal model for the analysis of spinal loading. PLoS ONE. **12**(1), (2017) https://doi.org/10.1371/journal.pone.0169329 . PLoS ONE **12**(1), e0169329

[30] Scovil, C.Y., Ronsky, J.L.: Sensitivity of a Hill-based muscle model to perturbations in model parameters. J. Biomech. **39**(11), 2055–2063 (2006) https://doi.org/10.1016/j.jbiomech.2005.06.005

[31] Ramsey, D.K., Crotin, R.L.: Stride length impacts on sagittal knee biomechanics in flat ground baseball pitching. Appl. Sci. **12**(3), 995 (2022) https://doi.org/10.3390/app12030995

[32] D'Hondt, L., De Groote, F., Afschrift, M.: A dynamic foot model for predictive simulations of human gait reveals causal relations between foot structure and whole-body mechanics. PLOS Comp. Bio. **20**(6), 1012219 (2024) https://doi.org/10.1371/journal.pcbi.1012219

[33] Falisse, A., Serrancolí, G., Dembia, C.L., Gillis, J., Jonkers, I., De Groote, F.: Rapid predictive simulations with complex musculoskeletal models suggest that diverse healthy and pathological human gaits can emerge from similar control strategies. J. R. Soc. Interface **16**(157), 20190402 (2019) https://doi.org/10.1098/rsif.2019.0402

[34] OpenSim Documentation: OpenSim::PointConstraint Class Reference. https://simtk.org/api_docs/opensim/api_docs/classOpenSim_1_1PointConstraint.html#details. Accessed: 2025-09-24 (2015)

[35] Liu, J.M., Knowlton, C., Gauthier, M., Tropp, Z., Verma, N., Nicholson, G., Zaferiou, A., et al.: Roles of each leg in impulse generation in professional baseball pitchers: preliminary findings uncover the contribution of the back leg towards whole-body rotation, 1–16 (2022) https://doi.org/10.1080/14763141.2022.2108490 . Advance online publication

[36] Dembia, C.L., Bianco, N.A., Falisse, A., Hicks, J.L., Delp, S.L.: OpenSim Moco: Musculoskeletal optimal control. PLoS Comp. Biol. **16**(12), e1008493 (2020). https://doi.org/10.1371/journal.pcbi.1008493

[37] Denton, A.N., Umberger, B.R.: Computational performance of musculoskeletal simulation in OpenSim Moco using parallel computing. Int. J. Numer. Method. Biomed. Eng. **39**(12), e3777 (2023). https://doi.org/10.1002/cnm.3777

[38] Werner, S.L., Fleisig, G.S., Dillman, C.J., Andrews, J.R.: Biomechanics of the elbow during baseball pitching. J. Orthop. Sports Phys. Ther. **17**(6), 274–278 (1993) https://doi.org/10.2519/jospt.1993.17.6.274

[39] Major League Baseball: Baseball Savant - Pitch arsenals leaderboard. Accessed: 2024-11-08 (2024). https://baseballsavant.mlb.com/leaderboard/pitch-arsenals

[40] Fortenbaugh, D., Fleisig, G.S., Andrews, J.R.: Baseball pitching biomechanics in relation to injury risk and performance. Sports Health **1**(4), 314–320 (2009) https://doi.org/10.1177/1941738109338546

[41] Anz, A.W., Bushnell, B.D., Griffin, L.P., Noonan, T.J., Torry, M.R., Hawkins, R.J.: Correlation of torque and elbow injury in professional baseball pitchers. Am. J. Sports Med. **38**(7), 1368–1374 (2010) https://doi.org/10.1177/0363546510363402

[42] Kageyama, M., Sugiyama, T., Takai, Y., Kanehisa, H., Maeda, A.: Kinematic and kinetic profiles of trunk and lower limbs during baseball pitching in collegiate pitchers. J. Sports Sci. Med. **13**(4), 742–750 (2014)

[43] Hakanson, S., Johnson, S.T., Norcross, E.C., Brown, C.N.: The effects of contralateral trunk tilt on elbow varus torque in baseball pitchers: A critically appraised topic. J. Sport. Rehabil. **30**(8), 1214–1219 (2021) https://doi.org/10.

1123/jsr.2020-0384

[44] Acosta, M.R., Van Ness, J.M., Lydon, W.P., Graham, B.G., King, A.C., Jensen, C.D.: Biceps and triceps contribute to pitching performance in college baseball. Med. Sci. Sports Exerc. **51**(6S), 65 (2019) https://doi.org/10.1249/01.mss.0000560688.68517.e9

[45] McCutcheon, T.W., Slowik, J.S., Fleisig, G.S.: Kinematic parameters associated with elbow varus torque in elite adult baseball pitchers. Orthop. J. Sports Med. **13**(2) (2025) https://doi.org/10.1177/23259671241300560

[46] Seiber, K., Gupta, R., McGarry, M.H., Safran, M.R., Lee, T.Q.: The role of the elbow musculature, forearm rotation, and elbow flexion in elbow stability: An in vitro study. J. Shoulder Elbow Surg. **18**(2), 260–268 (2009) https://doi.org/10.1016/j.jse.2008.08.004

[47] Fleisig, G.S., Andrews, J.R., Dillman, C.J., Escamilla, R.F.: Kinetics of baseball pitching with implications about injury mechanisms. Am. J. Sports Med. **23**(2), 233–239 (1995) https://doi.org/10.1177/036354659502300218

[48] Hicks, J.L., Uchida, T.K., Seth, A., Rajagopal, A., Delp, S.L.: Is my model good enough? Best practices for verification and validation of musculoskeletal models and simulations of movement. J Biomech. Eng. **137**(2), 020905 (2015) https://doi.org/10.1115/1.4029304

[49] Goislard de Monsabert, B., Rao, G., Gay, A., Berton, E., Vigouroux, L.: A scaling method to individualise muscle force capacities in musculoskeletal models of the hand and wrist using isometric strength measurements. Med. Biol. Eng. Comput. **55**(12), 2227–2244 (2017) https://doi.org/10.1007/s11517-017-1662-6

Appendix A Musculoskeletal Parameters for the OpenSim Forward Dynamic Model

All units are in degrees unless otherwise indicated. In this model, contralateral refers to motion towards the opposite side of the throwing (right) arm (i.e. to the left), while ipsilateral refers to motion towards the throwing side (i.e. to the right).

Degree of Freedom	Lower Bound (-)	Upper Bound (+)	Actuator Optimal Torque (N·m)	Initial Position
Pelvis Ipsilateral(+)/Contralateral(-) Tilt	-75	75	600	-11.1
Pelvis Clockwise(+)/Counterclockwise(-) Rotation	-90	90	600	-90.0
Pelvis Posterior(+)/Anterior(-) Tilt	-90	90	600	-6.6
Pelvis Posterior(+)/Anterior(-) Translation	0 m	1.1 m	650	0 m
Pelvis Superior(+)/Inferior(-) Translation	0.5 m	1.5 m	650	1.0 m
Pelvis Ipsilateral(+)/Contralateral(-) Translation	-0.3 m	0.3 m	650	0 m
Lumbar Ipsilateral(+)/Contralateral(-) Tilt	-75	75	500	-15
Lumbar Clockwise(+)/Counterclockwise(-) Rotation	-90	90	500	20
Lumbar Posterior(+)/Anterior(-) Flexion	-90	40	500	10
Right Hip Flexion(+)/Extension(-)	-45	120	750	28
Right Hip Adduction(+)/Abduction(-)	-60	40	750	4
Right Hip Internal(+)/External(-) Rotation	-90	90	750	14
Right Knee Extension(+)/Flexion(-)	-130	10	500	-30
Right Ankle Dorsiflexion(+)/Plantar Flexion(-)	-75	75	175	20
Right Ankle Inversion(+)/Eversion(-)	-50	50	150	0.6
Left Hip Flexion(+)/Extension(-)	-45	120	750	120
Left Hip Adduction(+)/Abduction(-)	-60	40	750	10
Left Hip Internal(+)/External(-) Rotation	-90	90	750	0
Left Knee Extension(+)/Flexion(-)	-130	10	500	-120
Left Ankle Dorsiflexion(+)/Plantar Flexion(-)	-75	75	175	0
Right Shoulder Horizontal Flexion(+)/Extension(-)	-40	90	450	40
Right Shoulder Abduction(+)/Adduction(-)	0	180	450	20
Right Shoulder Internal(+)/External(-) Rotation	-180	20	450	10
Right Elbow Flexion(+)/Extension(-)	0	130	350	120
Right Forearm Pronation(+)/Supination(-)	-90	90	350	90
Right Wrist Ulnar(+)/Radial(-) Deviation	-10	10	120	0
Right Wrist Flexion(+)/Extension(-)	-70	70	300	10
Left Shoulder Horizontal Flexion(+)/Extension(-)	-40	90	450	10
Left Shoulder Abduction(+)/Adduction(-)	0	180	450	10
Left Shoulder Internal(+)/External(-) Rotation	-180	20	450	10
Left Elbow Flexion(+)/Extension(-)	0	130	350	105
Left Forearm Pronation(+)/Supination(-)	-90	90	350	0
Left Wrist Ulnar(+)/Radial(-) Deviation	-10	10	300	0
Left Wrist Flexion(+)/Extension(-)	-70	70	120	0

Appendix B Diagram of the Forces and Torques of the Throwing Arm used to Formulate the UCL Loading Equation

.

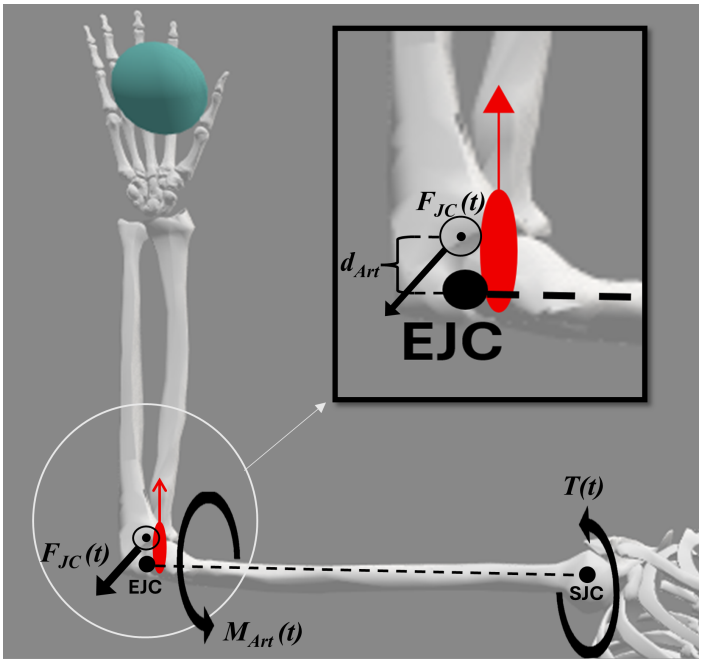

Fig. B1 Diagram of the forces and torques in the throwing arm used to formulate the UCL loading equation (Eq. (2)). EJC and SJC represent the elbow and shoulder joint centres, respectively. The dotted black line represents the humerus' longitudinal axis (varus–valgus). The red ellipsoid represents the UCL, while the red arrow is the UCL line of action. $T(t)$ is the shoulder rotation reserve actuator torque (valgus), while $M_{\mathrm{Art}}(t)$ is the varus moment, known as the osseous articulation or joint compression moment. d_{Art} is the moment arm from the joint centre to the medial edge of the elbow (radius), perpendicular to the varus–valgus axis of rotation, where the joint compression force ($F_{\mathrm{JC}}(t)$) acts. The joint compression force acts on the posterior elbow (in the direction out of the page), maintaining joint stability. This is denoted by black arrow originating at the circle with the dot in it (the circle is commonly used in circuit diagrams to specify current flow out of the page). The elbow joint compression force ($F_{\mathrm{JC}}(t)$), which acts along the anterior–posterior axis, creates a resultant varus moment ($M_{\mathrm{Art}}(t)$). Not to scale and made in OpenSim and edited in MS Word.

Appendix C Cost Function Used for Case 3

$$J = W_1 \left(\frac{v_{\text{ball, final}} - v_{\text{ball, desired}}}{v_{\text{ball, desired}}} \right)^2 + W_2 \left(\frac{v_{\text{foot, final}}}{v_{\text{foot, maximum}}} \right)^2 + W_3 \frac{1}{t} \int_0^t \left(\frac{M_{\text{UCL},-y}(\tau)}{M_{\text{ref}}} \right)^2 d\tau + \sum_{i=1}^{n_{\text{actuators}}} C_i \left(\frac{\text{actuation effort}_i}{\text{maximum effort}_i} \right)^2 \tag{3}$$

subject to

$$|v_{\text{ball, final}} - v_{\text{ball, desired}}| \leq 0.0001 \text{ m/s}$$
$$|v_{\text{foot, final}}| \leq 0.0001 \text{ m/s}$$
$$-1 \leq \text{controls}_{\text{ actuators}} \leq 1$$
$$0 \leq \text{controls}_{\text{ muscles}} \leq 1$$

where $W_1 = 15, \quad W_2 = 5, \quad W_3 = 1$

$$C_i = \begin{cases} 1, & \text{for the shoulder rotation actuator} \\ 0.001, & \text{otherwise} \end{cases} \qquad i = 1 \ldots n_{\text{actuators}}$$

$M_{\text{UCL},-y}(\tau)$ is the elbow joint *moment* about the varus–valgus axis
("$-y$" axis, where the negative represents valgus torque)
t is the motion duration (included for time-scale invariance)
M_{ref} is a normalization constant (e.g., peak elbow varus—valgus moment)
(the integral penalizes large values whenever they occur, not just at one instant)

Appendix D Right Toe Spherical Joint Connected to the Ground

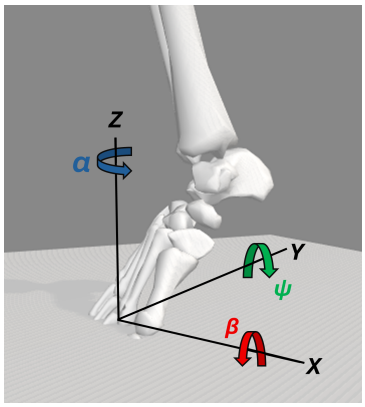

Fig. D2 Representation of the spherical joint, connecting a point on the distal end of the third metatarsal to the ground, that permits rotation (pivoting) about vertical z-axis (α), inversion/eversion about the y-axis (ψ), and heel lift about the x-axis (β).

Appendix E Ground Reaction Forces for Case 1

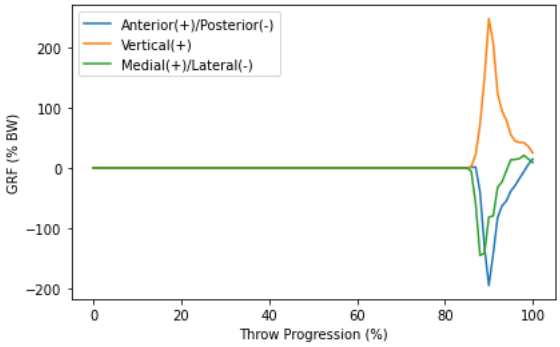

Fig. E3 Lead-foot heel contact sphere GRF of Case 1. GRFs were normalized to percentage of the model's body weight (BW), where 97.5 kg = 956.2 N of BW. On the horizontal axis, 0% corresponds to initiation of arm-cocking; 100% represents the instant of ball release. Developed in Python.

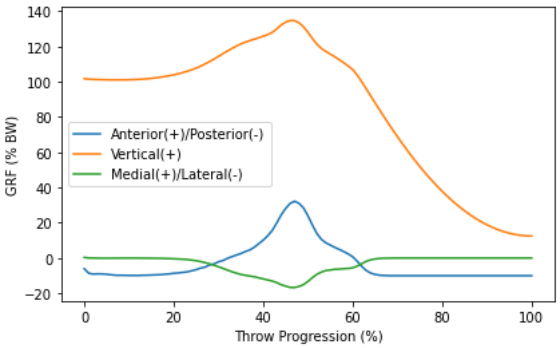

Fig. E4 Resolved components of the rear-foot GRF at the point constraint for Case 1. GRFs were normalized to percentage of the model's body weight (BW), where 97.5 kg = 956.2 N of BW. Along the horizontal axis, 0% corresponds to initiation of arm-cocking; 100% represents the instant of ball release. Developed in Python.

Appendix F Reserve Actuator Activation Across the Three Case Studies

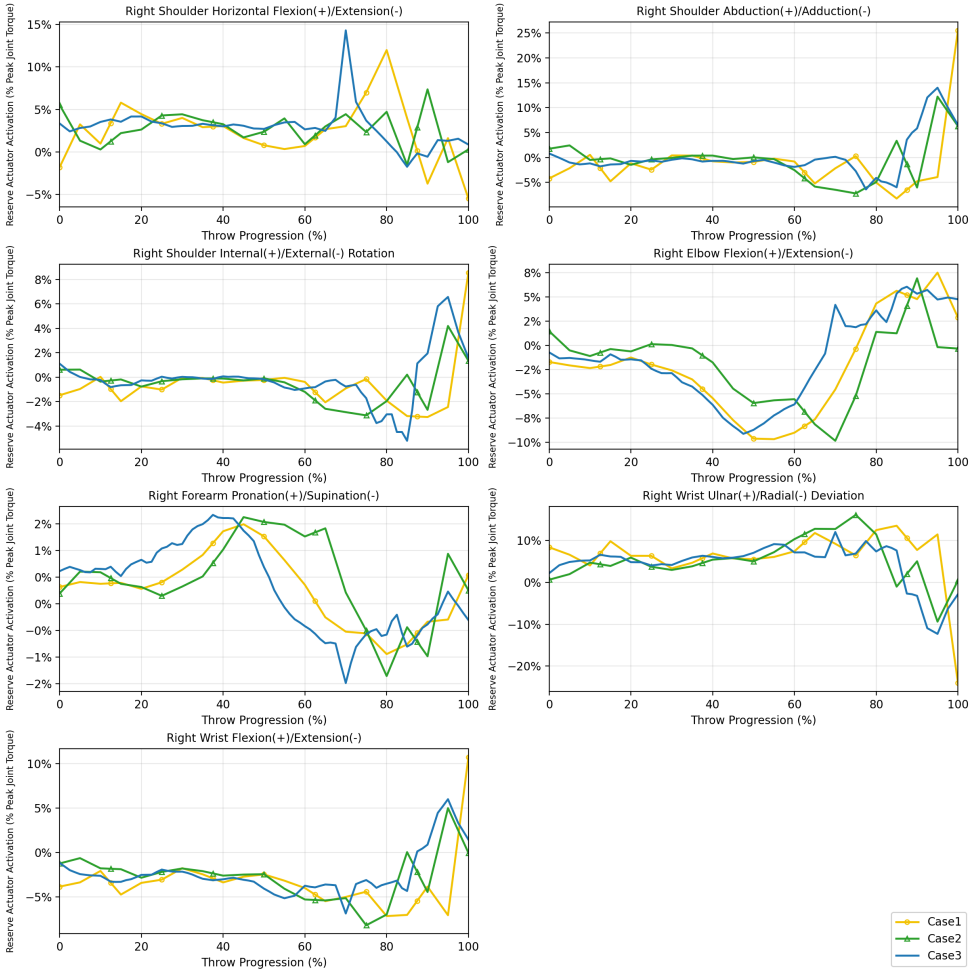

Fig. F5 Reserve actuator activation across the three case studies. On the horizontal axis, 0% corresponds to initiation of arm-cocking; 100% represents the instant of ball release. The vertical axis represents the reserve actuator activation as a percentage of the peak joint torque over the entire motion. Developed in Python.